Electronic structure, itinerant magnetism and orbital ordering of K_2NiF_4-type compounds

1993 J. Phys.: Condens. Matter 5 2987

(http://iopscience.iop.org/0953-8984/5/18/021)

J. Phys.: Condens. Matter 5 (1993) 2987–3002. Printed in the UK

Electronic structure, itinerant magnetism and orbital ordering of K_2NiF_4-type compounds

V Eyert† and K-H Höck‡

Institut für Festkörperphysik, Technische Hochschule Darmstadt, Hochschulstraße 6, 6100 Darmstadt, Federal Republic of Germany

Received 21 October 1992, in final form 15 February 1993

Abstract. We report on the first comprehensive theoretical study of the electronic, magnetic and structural properties of the quasi-two-dimensional magnetic insulators K_2NiF_4 and K_2CuF_4. Our investigations were carried out by means of electronic structure calculations based on density functional theory within the local density approximation, and led to full agreement with experiment with regard to many important ground-state properties. In particular they result in a correct description of the two-dimensional electronic dispersion, the insulating behaviour, the magnetic order and the structural distortions inherent in these compounds. We were also able to study the delicate interplay of all these properties. Furthermore we arrive at the conclusion that band theory is well suited to describe magnetic systems, which possess localized moments and serve as almost ideal candidates for the Heisenberg model.

1. Introduction

Magnetic insulators have long attracted interest, and still constitute a field of current research. This is due to many reasons, among which are interest in the purely magnetic properties of the insulators, and the investigation of the Mott–Hubbard metal–insulator transition.

A different, but likewise important, field of intense work may be summarized under the catchphrase 'low-dimensional systems'. Here one is faced with completely new problems intrinsic to the reduced dimensionality, which in many cases cannot be directly deduced from three-dimensional behaviour.

There exist in Nature ideal realizations of these extraordinary phenomena, in the form of a whole class of compounds with the general formula K_2MF_4, with M ranging from Mn to Cu. Representing in particular the two-dimensional case, they serve as traditional examples for this type of material and therefore have already entered into the textbooks [1]. The latter is due to the fact that these potassium compounds have been thoroughly investigated and thus many of their properties are now well known, at least from the experimental point of view [2].

The situation is different concerning our theoretical understanding. Here, the experimental observation of magnetic moments almost completely localized on the transition metal sites led to an approach based on an effective Heisenberg model. However, due to the two-dimensionality of these materials, one is then faced with the well known theorem,

† Present address: Max-Planck-Institut für Festkörperforschung, Heisenbergstraße 1, 7000 Stuttgart 80, Federal Republic of Germany.

‡ Present address: Institut für Theoretische Physik, Universität Augsburg, Memminger Straße 6, 8900 Augsburg, Federal Republic of Germany.

0953-8984/93/182987+16$07.50

formulated by Mermin and Wagner, which prohibits any long-range order in the two-dimensional isotropic model at finite temperatures [3]. Thus the question arose as to what type of exchange mechanism might govern the magnetism in these compounds.

In this paper we attack the problem in a different way and use a band picture, thereby aiming at a more complete understanding. We performed first-principles electronic structure calculations based on density functional theory (DFT) within the local density approximation (LDA), which also cover the electronic, magnetic and elastic degrees of freedom. The latter argument is an important aspect of the present investigation.

We started with the Ni and Cu compounds in this work, the latter being the only ferromagnet among the class K_2MF_4 mentioned above. The Ni system, in contrast, is the representative for the whole class that possesses the so-called K_2NiF_4 crystal structure, which is observed in many compounds.

Here we mention in particular La_2CuO_4, which has exactly this crystal structure at temperatures above 500 K [4] and is also an antiferromagnetic insulator. Furthermore, both systems exhibit an almost two-dimensional behaviour, conditioned by the crystal structure and showing up in many physical properties.

Finally, as is well known, La_2CuO_4 is directly connected to the high-T_c superconductors. In this context it was the subject of a wealth of electronic structure calculations which, in summary, led to the conclusion that none of the most common band structure methods based on density functional theory and the local density approximation is capable of properly describing the antiferromagnetic and insulating ground state and thereby go beyond the first results of Mattheiss [5]. The reasons for this failure now seem to be the strong electronic correlations, driving the transition to the antiferromagnetic insulator on the one hand, but putting density functional theory to a severe test on the other hand.

However, by going beyond traditional density functional theory, new calculations have succeeded in describing the correct ground-state properties of La_2CuO_4 in accordance with the experimental findings [6, 7].

Before turning to a description of our investigations of the compounds K_2NiF_4 and K_2CuF_4 we mention preliminary work [8, 9], which also reports on these compounds. In contrast to the present paper, emphasis in [8, 9] was placed more on the interrelation with high-T_c superconductivity; here, on the other hand, we will deal exclusively, and in far more detail, with K_2NiF_4 and K_2CuF_4. Furthermore, a renewed and profound analysis of the crystal structure data together with subsequent, more elaborate, calculations, has led to a qualitatively improved understanding of the underlying physical mechanisms.

The main body of this work is divided into three parts. In the following two sections we will summarize some of the experimental findings, and simply present the results of our calculations for K_2NiF_4 and K_2CuF_4, respectively. Their detailed discussion will be postponed to section 4, which will also deal with the interplay of magnetic and structural order. In section 5 we present a summary, and an outlook of future work.

2. K_2NiF_4

2.1. Experimental facts

The crystal structure of K_2NiF_4 consists of a body-centred tetragonal (BCT) lattice with the space group D_{4h}^{17} and the atoms arranged as shown in figure 1 [10–12].

Worth mentioning in this structure are the NiF_6 octahedra, stressing the intimate relationship with the cubic perovskites. In the latter, their three-dimensional interconnection essentially maintains the high mechanical stability, whereas in K_2NiF_4 the decoupling of the

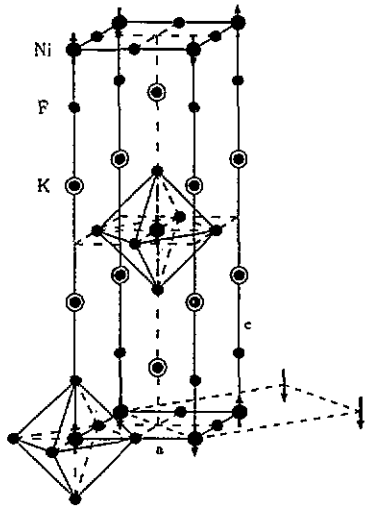

Figure 1. Body-centred tetragonal crystal structure of K_2NiF_4. Drawn in are the lattice constants, the atomic positions and the directions of the magnetic moments localized at the Ni sites. The broken lines indicate the basal plane of the side-centred orthorhombic cell (see text).

octahedra along the c direction limits this stability to the NiF_2 planes and thereby leads to the typical layer structure, which shows up in the two-dimensional electronic and magnetic behaviour of this and similar systems.

We should also mention the flattening of the octahedra of around 1% along the c direction, i.e. the distance between the Ni ion and the apical F ion is shorter by this amount than the corresponding in-plane distances [10, 11]. This seems to be typical for all compounds having this structure [13, 14]. The crystal structure data are collected in table 1 [12], which furthermore serves as a starting point for the band structure calculations.

Table 1. Structural data for BCT K_2NiF_4 [12].

Space group	D_{4h}^{17} / *I4/mmm*
Lattice constants	$a = b = 3.994$ Å, $c = 13.04$ Å
Positions	Ni: (0,0,0) F: $(\frac{1}{2}, 0, 0)$, $(0, \frac{1}{2}, 0)$, $(0, 0, z_F)$, $(0, 0, -z_F)$ K: $(0, 0, z_K)$, $(0, 0, -z_K)$
Parameters	$z_F = 0.152$, $z_K = 0.352$

Concerning the magnetism, the well localized Ni moments order at a Néel temperature of $T_N = 97.23$ K with a spin alignment as indicated in figure 1 [12, 15]. The static $T = 0$ moment amounts to $2.22\mu_B$, as measured by antiferromagnetic resonance [12].

In their investigation of the underlying exchange mechanisms Birgeneau and co-workers found long-range magnetic correlations in the NiF_2 planes at temperatures from 200 K down to approximately 100 K, but no inter-plane couplings [12, 16–18]. At T_N, K_2NiF_4 exhibits a very sharp phase transition to a long-range three-dimensional magnetic order which, however, is still of mainly two-dimensional character. This was supported by measurements

of the spin-wave spectrum at 5 K, which lacked any dispersion along the [001] direction [17, 18].

All these experimental findings suggested describing K_2NiF_4 by a two-dimensional effective ($S = 1$) Heisenberg model, whose Hamiltonian contains the indirect superexchange between localized in-plane Ni moments but to be extended by an Ising-like anisotropy, as proposed by Lines [19]. This anisotropy is responsible for the alignment of the magnetic moments along the c axis, and consists of a dipole–dipole and a crystal field contribution.

Birgeneau and co-workers gave a value of $J/k_B \approx -100\,K$ for the in-plane exchange constant [12], and estimated the inter-plane exchange constant to be $J' < -0.0037J$ from their spin-wave measurements [17].

2.2. *Band structure results*

Turning to a discussion of our electronic structure calculations, we begin with a few technical remarks. The calculations were performed using the ASW method [20] in its scalar relativistic implementation [21, 22], and they were all carried to full self-consistency.

Since the antiferromagnetic state cannot be described within the above-mentioned BCT cell, which contains only one formula unit, we had to pass over to a site-centred orthorhombic (SCO) lattice, as already indicated in figure 1 by broken lines. The latter may be constructed from the BCT cell by rotating the a and b axes by 45° around the z axis and stretching them by a factor of $\sqrt{2}$ while keeping the c axis fixed. It allows for two formula units, and thus for the inclusion of both magnetic sublattices. Nevertheless, we started our calculation for the non-magnetic configuration within the chemical unit cell.

In the same manner as the LMTO method [23] the ASW method uses atomic spheres, the radii of which are fixed by the condition that the sum of the atomic sphere volumes equals the volume of the whole cell. In order to arrive at physically reasonable ratios of the radii in the layer structure of K_2NiF_4, we followed a well known recipe to deal with open structures [24] and inserted empty spheres at the following positions:

$$E_1 : (\tfrac{1}{2}, \tfrac{1}{2}, 0) \qquad E_2 : (\tfrac{1}{2}, 0, \pm z_F), (0, \tfrac{1}{2}, \pm z_F).$$

This then allowed us to fix the atomic sphere radii to $2.602\,28 a_B$ for the potassium and the apical fluorine, and $2.297\,92 a_B$ for all the other spheres.

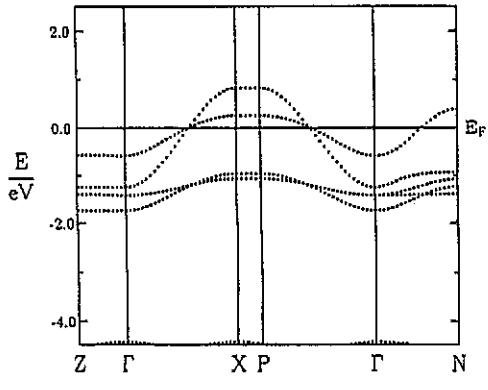

Figure 2. Band structure of non-magnetic K_2NiF_4 in the BCT-structure.

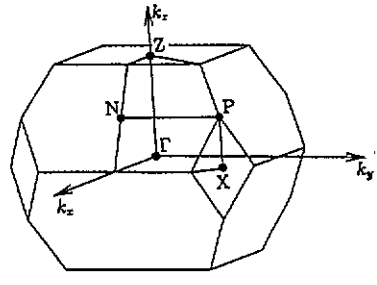

Figure 3. Brillouin zone of the BCT lattice.

To present the results we begin with the band structure of non-magnetic K_2NiF_4 in the BCT structure, as shown in figure 2. The symmetry lines depicted there connect the points highlighted in figure 3. In figure 2 we identify the Ni d-bands around the Fermi energy. They lie in an energy gap of approximately 8 eV separating the F p-bands (which are still visible at the bottom of the picture) and the K s-bands. The d bands separate in the lower t_{2g} bands and the e_g bands due to crystalline symmetry. Concerning the latter, we may further distinguish the $d_{x^2-y^2}$ from the d_{z^2} band, which is the highest state at the Γ point.

Finally, we mention the almost totally vanishing dispersion along the line Γ–Z, which reflects our expectation, discussed above, of the effects of two-dimensionality.

It is interesting to compare these results with those for La_2CuO_4 [5]. The differences between the electronic structures of K_2NiF_4 and La_2CuO_4 are simply stated [8, 9]. Though it is still possible to identify the transition-metal d states in the latter system, especially the $d_{x^2-y^2}$ state crossing the Fermi level and the d_{z^2} band lying below E_F due to the increased number of valence electrons, there is a strong hybridization of Cu d-states and O p-states. This results in a wide complex of d and p bands, which furthermore shows a finite dispersion along the z axis. Common to both systems, however, is the characteristic crossing of the Fermi level in the middle of the line Γ–X.

Concentrating again on K_2NiF_4, it is exactly this feature that plays an important role in the transition to the antiferromagnetic insulator. To see this we will first turn to the side-centred orthorhombic structure mentioned above. Its Brillouin zone is depicted in figure 4, and figure 5 shows how it is embedded in the Brillouin zone of the BCT lattice. In figure 5 we see that the points labelled X_1 and X_2 in the BCT zone turn out to be the Z and Γ point in the SCO zone. Furthermore, all states on the hexagonal surfaces of the latter will be doubly degenerate.

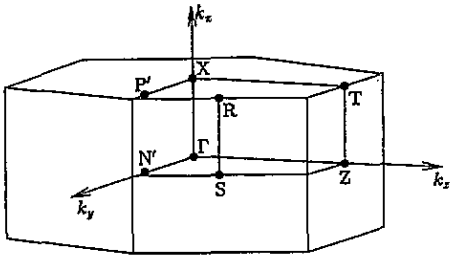

Figure 4. Brillouin zone of the SCO lattice. Points P' and N' refer to $(\frac{1}{2}, \frac{1}{2}, 0)$ and $(0, \frac{1}{2}, 0)$, respectively.

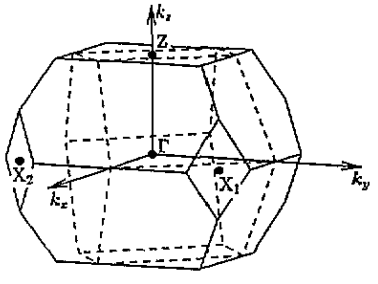

Figure 5. Brillouin zones of the BCT (full lines) and the SCO (broken lines) lattices.

This is confirmed by the band structure for non-magnetic K_2NiF_4, calculated within the SCO structure and shown in figure 6. There we can clearly see that the bands between the points Γ and X in the SCO zone originate from folding back the bands between $(\frac{1}{4}, \frac{1}{4}, 0)$ and $X = X_2 = (\frac{1}{2}, \frac{1}{2}, 0)$ to the bands between $(\frac{1}{4}, \frac{1}{4}, 0)$ and Γ in the BCT zone, thereby yielding a double degeneracy at X (SCO).

This degeneracy may be lifted by an antiferromagnetic order, as we can tell from figure 7, which shows the band structure corresponding to this case and where an energy gap of 0.8 eV at the Fermi energy clearly classifies K_2NiF_4 as an antiferromagnetic insulator. The same calculation yields a magnetic moment of $1.34\mu_B$ and $1.23\mu_B$ per sublattice and Ni atom, respectively. The latter is almost entirely due to the Ni d-states, which are occupied

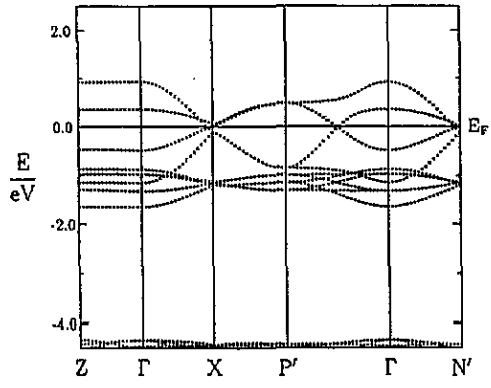

Figure 6. Band structure of non-magnetic K_2NiF_4 in the SCO structure.

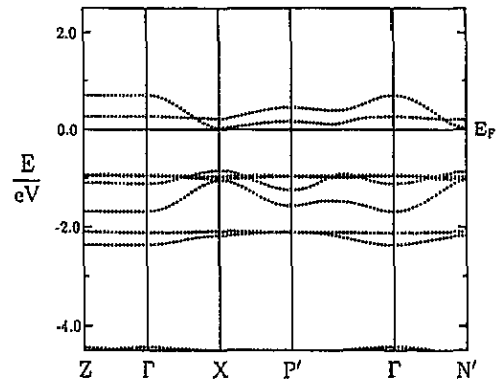

Figure 7. Band structure of antiferromagnetic K_2NiF_4 in the SCO structure.

by about 8.2 electrons. A comparison of the total energies reveals a stability of 24 mRyd of the antiferromagnetic solution relative to the non-magnetic solution.

Unfortunately there are no BIS or UPS measurements, known to us, to which our value for the energy gap at the Fermi level could be compared. However, we are able to confirm the value of 0.936 eV for the crystal field splitting of the Ni d-states, as found by Tiwari and co-workers [25]. Inspection of our partial Ni d density of states yields around 0.9 eV.

We can thus summarize our results on K_2NiF_4 to the effect that electronic structure calculations confirm well the experimentally observed ground-state properties. This statement covers electronic configurations and energies, in particular the vanishing density of states at the Fermi energy and finally stable magnetic order and moments, albeit with deviations concerning the latter.

3. K_2CuF_4

3.1. Experimental facts

The quasi-two-dimensional system K_2CuF_4 is the only ferromagnet among all the antiferromagnets of the series K_2MF_4 with M = Mn, ..., Cu. It has thus attracted particular attention for some time, especially in view of the many similarities among the class K_2MF_4 [2]. By the latter we mean, as well as the magnetic order due to localized moments, the common crystal structure based on a body-centred tetragonal lattice and the unit cell shown in figure 1, even if K_2CuF_4 possesses just a slight orthorhombic distortion, which we will discuss later.

Concerning the magnetism, K_2CuF_4 belongs to the relatively young class of ferromagnetic insulators [26], its Curie temperature being $T_c = 6.25$ K [27, 28]. The moments are again well localized on the transition-metal sites, this time aligned perpendicular to the c axis and having a value of exactly $1.0\mu_B$ at T = 0 [27–29]. Finally, spin-wave measurements again reveal long-range magnetic correlations above T_c and a quasi-two-dimensional magnetic order at low temperatures. This has been concluded from the lack of magnon dispersion along the c axis [30].

A description with the help of the two-dimensional Heisenberg model extended by an anisotropy term as in the case of K_2NiF_4 will certainly not suffice here, since there is only

an XY-like anisotropy of about 1% [27, 28, 31, 32]. The latter, however, also comes under the validity of the Mermin–Wagner theorem.

It seems likely that in K_2CuF_4 the inter-plane exchange alone stabilizes the magnetic order, even if it is still very small compared to the in-plane exchange; experimental values are $J' = 0.000\,66J$ and $J/k_B = 11.4\,K$ [28].

The discussion of ferromagnetic order in K_2CuF_4 directly leads to the above-mentioned orthorhombic distortion, since both are intimately connected. This has been pointed out first by Khomskii and Kugel [33, 34]. The connection traces back to the existence of ions with orbitally degenerate states in magnetic insulators, which results in an interesting interplay of the magnetic and orbital order.

A typical example for such behaviour was long held to be Cu^{2+} ions in an octahedral surrounding. Without distortions the two degenerate e_g states lie above the three t_{2g} orbitals. Experience has shown that this situation should lead to an elongation of the octahedron, i.e. to four short and two long Cu^{2+} ligand distances. This was indeed observed in all Cu compounds in question, until Knox reported the opposite situation in K_2CuF_4 [35]. There he found a compression of the distance between the Cu ion and the apical F ion of about 6% compared to the other four in-plane distances. His results were later confirmed by Yamada and by Hirakawa and Ikeda [27, 28].

In order to resolve the discrepancies between the Knox results on K_2CuF_4 and the experimental findings on many other Cu systems, Khomskii and Kugel in their theoretical study extended the conventional superexchange model to account for magnetic ions with orbital degeneracies. Concentrating on K_2CuF_4 led the authors to the following conclusions [33, 34]. *First, the crystal structure containing compressed octahedra as reported by Knox* was shown to be incompatible with the observed ferromagnetic order when the experimental exchange constants were used. Second, starting from ferromagnetism led to an alternating occupation of either the $d_{z^2-x^2}$ or the $d_{z^2-y^2}$ orbital when going from one in-plane Cu site to the next. This orbital order, however, requires the presence of two different distortions of the CuF_6 octahedra, which occur alternately and energetically favour either the former or the latter orbital.

These findings finally caused Khomskii and Kugel to propose an antiferrodistortive structure for K_2CuF_4, as shown in figure 8 in which the in-plane F ions are shifted from their position centred between the Cu ions. The region within the full lines in figure 8 corresponds to the area of the basal plane of the SCO unit cell which was highlighted by broken lines in figure 1. The bigger SCO cell with two formula units must now be used, due to the crystal structure distortion which lifts the BCT symmetry.

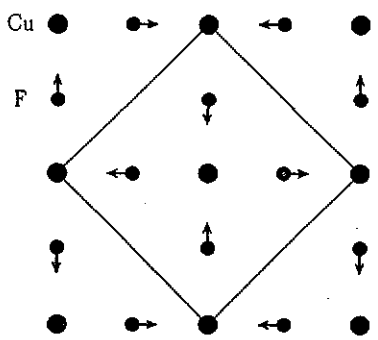

Figure 8. Distortion pattern of the basal plane in K_2CuF_4. Full lines mark the edges of the orthorhombic unit cell.

Worth mentioning about the distorted crystal structure is the fact that the CuF_6 octahedra are not compressed along the z axis, as reported by Knox, but are rather elongated alternately in the x and y direction. In effect, this means a coupling of the distortions of neighbouring octahedra.

The results of Khomskii and Kugel initiated a second period of experimental work on the crystal structure of K_2CuF_4 resulting in a clear-cut confirmation of their theoretical prediction [29, 32, 36, 37]. The measurements yielded a side-centred orthorhombic lattice with space group D_{2h}^{18}, and an alternating elongation of the octahedra within the planes of about 15%, corresponding to a shift of the fluorine ions of 2.5% of the lattice constant. Finally, they revealed the equality of the other four respective Cu–F distances in the octahedra. These results thus re-established the common experience that the octahedra should be elongated.

As in the case of K_2NiF_4 we have collected the exact experimental results [32] in form of a table: table 2 corresponds to the *fictitious* BCT crystal structure and serves as a comparison with table 1, whereas table 3 contains the correct SCO structure based on the experimental data [32].

Table 2. Structural data for (fictitious) BCT K_2CuF_4.

Lattice constants	$a = b = 4.1475$ Å, $c = 12.734$ Å
Positions	Cu: (0,0,0) F: $(\frac{1}{2}, 0, 0)$, $(0, \frac{1}{2}, 0)$, $(0, 0, z_F)$, $(0, 0, -z_F)$ K: $(0, 0, z_K)$, $(0, 0, -z_K)$
Parameters	$z_F = 0.1523$, $z_K = 0.3568$

Table 3. Structural data for SCO K_2CuF_4 according to [32].

Space group	D_{2h}^{18} / *Cmca*
Lattice constants	$a = b = 5.8655$ Å, $c = 12.734$ Å
Positions	Cu: $(0, 0, 0)$, $(\frac{1}{2}, \frac{1}{2}, 0)$ F: $(\frac{1}{4} - \delta, \frac{1}{4} - \delta, 0)$, $(\frac{1}{4} + \delta, \frac{3}{4} - \delta, 0)$, $(\frac{3}{4} - \delta, \frac{1}{4} + \delta, 0)$, $(\frac{3}{4} + \delta, \frac{3}{4} + \delta, 0)$, $(0, 0, \pm z_F)$, $(\frac{1}{2}, \frac{1}{2}, \pm z_F)$ K: $(0, 0, \pm z_K)$, $(\frac{1}{2}, \frac{1}{2}, \pm z_K)$
Parameters	$z_F = 0.1523$, $z_K = 0.3568$, $\delta = 0.01758$

3.2. Band structure results

Turning again to the calculations, we first note that they were conducted in exactly the same manner as those for the Ni system. The only exception consists of a different choice of the atomic sphere radii: we used $2.4a_B$ for the Cu atoms, $2.687\,36a_B$ for the potassium and the apical fluorine, and $2.3a_B$ for the in-plane fluorine and the empty spheres.

We started the calculations by making use of the fictitious BCT crystal structure, showing the resulting band structure in figure 9, where we choose the same energy window and symmetry lines as in the corresponding band structure of K_2NiF_4 (figure 2). First, we recognize again the five d bands in the middle of the figure and at the lower edge the fluorine p bands. Comparing both figures we note the different position of the d bands relative to the Fermi level, which can be simply explained by the increased electron number.

Furthermore, we see a shift of the F p-bands, which diminishes the gap between the d and p states. Nevertheless, there is still a separation of about 1 eV, opposite to the situation in La_2CuO_4.

As a next step we turn to the SCO crystal structure but first neglect the distortion of the octahedra, i.e. we start with $\delta = 0$ in the notation of table 3. For this case figure 10 shows the electronic structure as grown out of a non-magnetic calculation which, as explained in connection with figure 6 for K_2NiF_4, may be constructed directly from the band structure for the BCT lattice by folding the bands to the SCO Brillouin zone. It thus merely serves as a clue for the results of a subsequent ferromagnetic calculation, which yields a magnetic moment of $0.49\mu_B$ and $0.75\mu_B$ per Cu ion and formula unit, respectively. Furthermore, we get for this case a total energy that is 1.5 mRyd below the value of the non-magnetic calculation. The band structure is given in figure 11 and shows an almost rigid shift of the spin-up and spin-down bands away from their position in figure 10. However, it lacks the experimentally observed energy gap at the Fermi level.

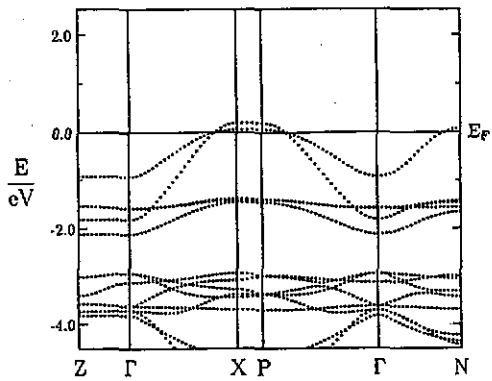

Figure 9. Band structure of non-magnetic K_2CuF_4 in the BCT structure.

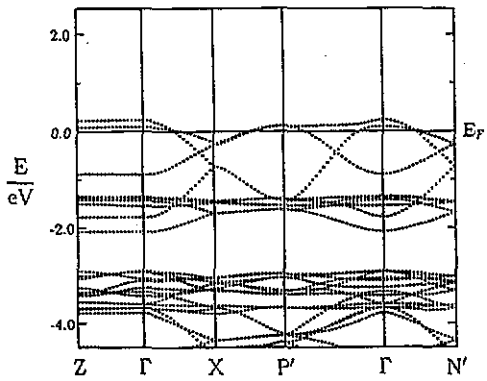

Figure 10. Band structure of non-magnetic K_2CuF_4 in the SCO structure.

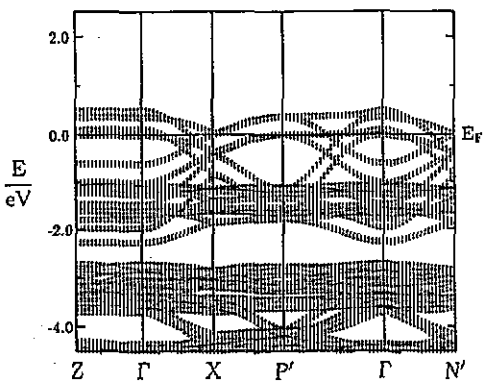

Figure 11. Band structure of ferromagnetic K_2CuF_4 in the SCO structure. Arrows denote spin-up and spin-down bands.

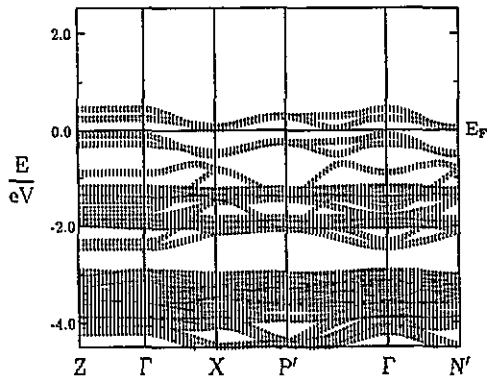

Figure 12. Band structure of ferromagnetic K_2CuF_4 in the SCO structure with $\delta = 0.01758$.

This changes when we use the experimental data given in table 3, i.e. when we include the octahedral distortion, $\delta = 0.017\,58$. In this case we get a vanishing density of states at the Fermi level and thus the insulating ground state of this compound. This goes along with a further decrease of the total energy down to 10 mRyd below the value of the non-magnetic calculation for this value of δ. The magnetic moment, on the other hand, increases to $0.66\mu_B$ per Cu ion and is carried alone by the 9.1 d electrons. Per formula unit we get a value of exactly $1.0\mu_B$, which is fixed to an integer value due to the existence of the gap at the Fermi energy. The band structure for this, real, situation is shown in figure 12.

To summarize these results, we are thus able to confirm important experimental observations in the same manner as for K_2NiF_4. Here again we mention the electronic configurations, the electronic structure, the insulating ground state and finally the stable magnetic order and moments, which come out in perfect agreement with the experimental findings.

Beyond these results we have now benefited from the fact that our approach includes the different degrees of freedom on the same footing, since this opened the way to the experimentally observed ferromagnetic insulator simply by shifting the atoms to their correct positions.

The necessity of such an approach for a correct description of the properties of K_2CuF_4 had already been clearly demonstrated by Khomskii and Kugel. In that respect our method is similar to their model. Concerning the results, however, we have some differences. According to Khomskii and Kugel the observed ferromagnetic order is incompatible with the orbital and crystal structure assumed by Knox, i.e. the regular structure without deviations from tetragonal symmetry and a filled d_{z^2} orbital. Against that we have found exactly for this structure a stable ferromagnetic solution, which is demonstrated by figure 11.

Our calculations further lead to the following conclusion. When going from figure 11 to figure 12, which merely corresponds to switching on the orthorhombic distortion, we clearly note the transition from the metallic to the insulating state. Consequently it is the insulator that is in contrast to the tetragonal crystal structure and *not* the ferromagnetic order.

4. Crystal structure and magnetic order

In the present section we will undertake a systematic investigation covering a wide range of phenomena inherent in the Cu as well as the Ni compound, and thereby aim at an interpretation of their physics on a common basis. In particular this will enable us to study the interplay of electronic conductivity, magnetic order and deviations from the regular tetragonal crystal structure, as shown in figure 1.

For this purpose we performed many self-consistent electronic structure calculations for both systems. They covered non-magnetic, ferromagnetic and antiferromagnetic configurations and octahedral distortions ranging from $\delta = 0$ to $\delta = 0.03$. The main results are collected in figures 13 and 14 for K_2NiF_4 and K_2CuF_4, respectively. In these figures we have limited the representation to only three different distortions ($\delta = 0$, $\delta = 0.01$ and $\delta = 0.017\,58$, the latter being the experimental distortion of K_2CuF_4) and furthermore to a small energy window and two lines ($P' \rightarrow \Gamma \rightarrow X$) of the SCO first Brillouin zone, figure 4. Note that figure 13 contains only two columns, because no ferromagnetic solution could be found. Furthermore, it should be pointed out that figure 13(*a*), (*b*) and figure 14(*a*), (*b*), (*f*) are simply sections of the previously shown figures 6, 7, 10–12.

Looking first at K_2NiF_4, we recognize the transition from the non-magnetic metal to the antiferromagnetic insulator when going from figure 13(*a*) to (*b*). However, we likewise

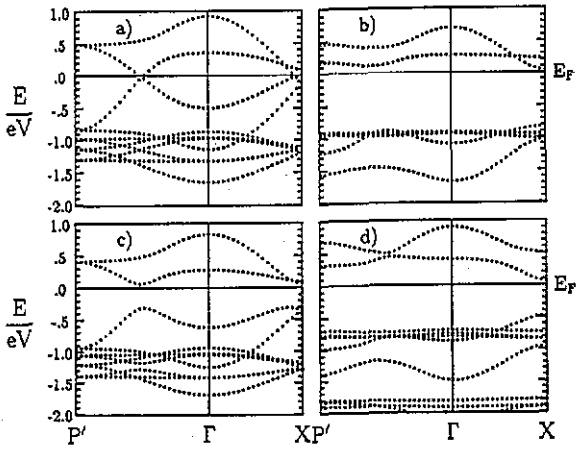

Figure 13. Band structures of K_2NiF_4 in the SCO structure for different distortions as resulting from non-magnetic and antiferromagnetic calculations, respectively; (a) $\delta = 0.0$, non-magnetic, (b) $\delta = 0.0$, antiferromagnetic, (c) $\delta = 0.01$, non-magnetic, (d) $\delta = 0.01$, antiferromagnetic.

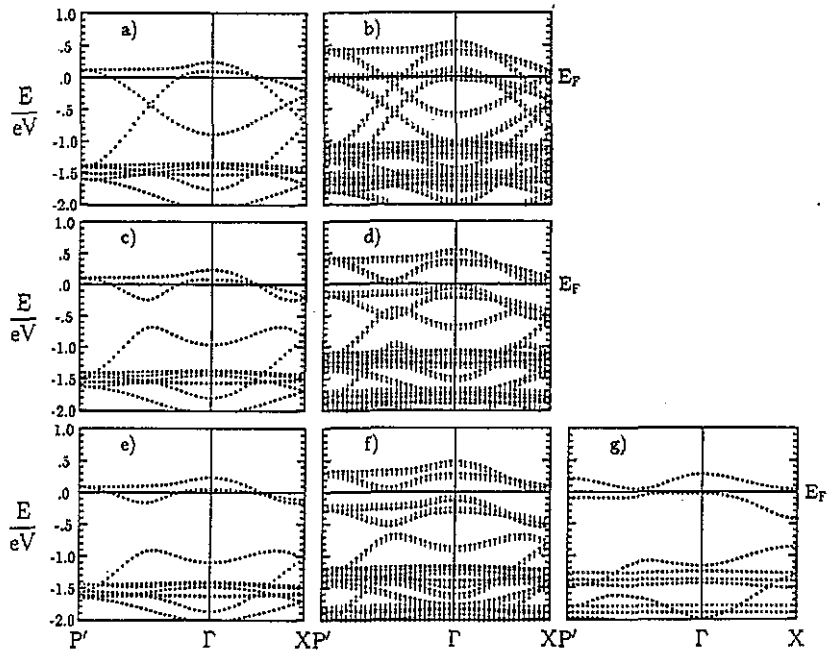

Figure 14. Band structures of K_2CuF_4 in the SCO structure for different distortions as resulting from non-magnetic, ferromagnetic and antiferromagnetic calculations, respectively; (a) $\delta = 0.0$, non-magnetic, (b) $\delta = 0.0$, ferromagnetic, (c) $\delta = 0.01$, non-magnetic, (d) $\delta = 0.01$, ferromagnetic, (e) $\delta = 0.01758$, non-magnetic, (f) $\delta = 0.01758$, ferromagnetic, (g) $\delta = 0.01758$, antiferromagnetic.

realize that a gap opens at the Fermi energy when we imprint an antiferrodistortive structure, i.e. when we go from figure 13(*a*) to (*c*). The origin of this gap in both cases lies in the

characteristic crossing of the two original $d_{x^2-y^2}$ bands, which can be traced back to the band crossing the Fermi level along the symmetry line Γ–N in figure 2 when remembering the backfolding procedure outlined in section 2 and the almost vanishing dispersion along the z direction. Thus when going from the BCT cell to the SCO cell we get a degeneracy of the 'old' $d_{x^2-y^2}$ band, which can be lifted by breaking the tetragonal crystal symmetry. This may be achieved by an antiferromagnetic or likewise an antiferrodistortive order, as figure 13(*b*) and (*c*) show. Taking into account both of them, which corresponds to figure 13(*d*), does not alter the situation substantially. It should be noted that, since the degenerate states in figure 13(*a*) are located at the Fermi level, a very small distortion is already sufficient to make K_2NiF_4 an insulator (see figure 13(*b*), (*c*)).

This is different in K_2CuF_4. Indeed here the d bands have almost the same shape as in the Ni compound, as we have already realized when comparing the figures 2 and 9, or 13(*a*) and 14(*a*), respectively. Even so, we are now faced with a higher number of electrons, which causes an almost rigid band shift of about 0.5 eV. Consequently the energy gap opening, when the distortion is switched on, lies by exactly the same amount *below* the Fermi energy. This is confirmed upon inspection of figures 13(*c*) and 14(*c*). Furthermore, the spin-degenerate band, which is seen to cross the Fermi level in figure 14(*c*), is half-filled and thus prevents the system from becoming an insulator, independent of the distortion strength δ. This argument is supported by figure 14(*e*) where the band, though having become narrower, is still pinned to the Fermi level. Our calculations acknowledge this fact by a steady increase of the density of states at E_F.

Things change when we break the spin-symmetry and allow for a ferromagnetic order. This causes the bands to be split, but still does not produce any gap (see figure 14(*b*)). Only when we lift the tetragonal symmetry of the crystal as well, and furthermore decrease the dispersion of the bands near the Fermi energy by increasing the distortion parameter δ, do we get the ferromagnetic insulator shown in figure 14(*f*). Thus, in contrast to K_2NiF_4, neither the lattice distortion nor the magnetic order alone are sufficient to produce a gap at the Fermi energy. Instead we need both of them.

This observation completes the discussion started at the end of section 3, where we had seen that the orthorhombic distortion is a prerequisite for the insulating ground state and that ferromagnetic order may be realized within the tetragonal structure. Now we come to the conclusion that both magnetism and orthorhombic distortion have to be required in order to arrive at the insulating ground state.

Finally, in figure 14(*g*) we add the band structure of fictitious antiferromagnetic K_2CuF_4, which also shows a gap at E_F.

From the above investigation alone it is not yet obvious which type of magnetic order comes into question for K_2CuF_4, since both the ferromagnetic and the antiferromagnetic solution as given in figures 14(*f*) and (*g*) show a gap. In order to rule out one of them we have to compare to the very end their total energies.

We therefore calculated, in general, for each value of the distortion parameter δ within the range mentioned at the beginning, the total energies of different magnetic structures. The results are depicted in figure 15, where we have given the total energy difference of the two most stable (non-magnetic, ferromagnetic, or antiferromagnetic) solutions for each δ and added the corresponding curve for the Ni system. Note that this *a priori* does not allow for a direct comparison of the results for different values of δ. However, both curves reflect in a clear-cut manner the experimental findings and complete our theoretical picture as drawn on the preceding pages by yielding the maximum magnetic energy gain for the undistorted structure of K_2NiF_4 and for a value of δ that is near to the experimental value of $\delta = 0.01758$ in the case of K_2CuF_4.

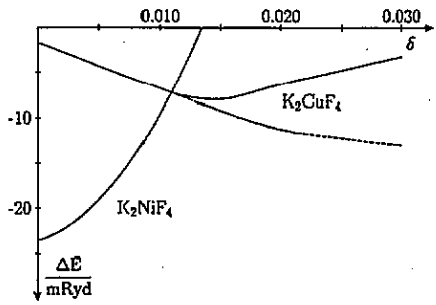

Figure 15. Total energy differences as a function of the in-plane distortion in the sco unit cell. For K_2NiF_4 the energy difference $\Delta E(\delta) = E_{af}(\delta) - E_{non}(\delta)$ is shown, where $E_{xx}(\delta)$ is the total energy of the respective configuration at a certain δ. The full curve marked K_2CuF_4 corresponds to $\Delta E(\delta) = E_{fe}(\delta) - E_{non}(\delta)$ for $\delta \leqslant 0.01$ and $\Delta E(\delta) = E_{fe}(\delta) - E_{af}(\delta)$ for $\delta \geqslant 0.01$. The broken curve gives $\Delta E(\delta) = E_{fe}(\delta) - E_{non}(\delta)$ for $\delta \geqslant 0.01$ for K_2CuF_4.

For later discussion we complement the total energy difference curves with some remarks about the magnetization (per formula unit or sublattice, respectively). In the case of K_2NiF_4 the magnetic moment amounts to $1.34\mu_B$ at $\delta = 0$, as already mentioned. It decreases as δ increases to a value of $1.01\mu_B$ at $\delta = 0.015$, hence near the point where the antiferromagnetic solution becomes unstable.

Concerning the Cu compound, we noted in section 3 that the magnetic moment starts with $0.75\mu_B$ at $\delta = 0$ and increases as the distortion is turned on, reaching $1.0\mu_B$ at approximately $\delta = 0.005$ where the gap opens. For antiferromagnetic K_2CuF_4 our calculations yielded an increase from $0.82\mu_B$ at $\delta = 0.015$ to $0.93\mu_B$ at $\delta = 0.030$.

In order to begin a discussion of all these results we first note again that the electronic structures of both compounds are nearly the same, as a comparison of figures 13(*a*), (*c*), (*d*) and the respective figures 14(*a*), (*c*), (*g*) reveals. Hence the higher electron number in K_2CuF_4 merely results in an almost rigid shift of the bands relative to the Fermi energy. It seems to be this shift alone that accounts for the fact that, for K_2NiF_4, antiferromagnetism is most stable within the tetragonal structure, whereas in the Cu compound the ferromagnetic state tends to prefer a finite orthorhombic distortion.

As we have already seen in connection with figure 13, in K_2NiF_4 both the antiferromagnetic as well as the antiferrodistortive order are equivalent insofar as they both imprint a modulation described by the same q vector, thereby opening the gap. Due to this equivalence antiferromagnetic order becomes more and more unstable against an antiferrodistortive structure as δ increases, and finally will be defeated even if there still exists an appreciable magnetic moment. In addition we note that the energy gain due to the above-mentioned Fermi-surface instability cannot be realized within a ferromagnetic structure, which therefore seems to be energetically unfavourable.

Though the same mechanism is also present in K_2CuF_4 its effect is only of secondary importance here since the gap opened by this instability lies 0.5 eV below the Fermi level. Instead we are faced here with another instability against a mode, which corresponds to switching on both the distortion and antiferromagnetism. Thus in K_2CuF_4 there is a collaboration of these two mechanisms rather than a competition as in the Ni compound. This different behaviour results exclusively from the Fermi-surface shift due to the increased electron count. Moreover, from these arguments it is clear that antiferromagnetism will be favoured energetically in the Cu system in the course of the orthorhombic distortion, as we can tell from the corresponding energy gain (which is the difference of the full and broken

curve above $\delta = 0.01$ in figure 15).

We are still faced with the question of why there is ferromagnetic rather than antiferromagnetic order in K_2CuF_4. In our opinion this cannot be answered in a clear-cut manner, but rather results from comparison of the total energies. However, there is a strong argument for ferromagnetism. By this we mean the already-mentioned existence of a spin-degenerate band pinned to the Fermi energy of the non-magnetic solution and leading to a steady increase of the density of states at E_F when going from figure 14(*a*) to (*e*), i.e. increasing the distortion parameter δ. Hence, according to the Stoner criterion, ferromagnetic order becomes increasingly likely and stable when shifting the atoms. This is indeed our observation in figure 15, as can be seen from the full and broken curve below and above $\delta = 0.01$, respectively.

In summary the orthorhombic distortion in K_2CuF_4 supports both ferromagnetic as well as antiferromagnetic order (albeit via different mechanisms) and it is not *a priori* obvious which of them wins. However, it might be argued that ferromagnetism already exists at $\delta = 0$ and thus has a certain advantage.

5. Summary and outlook

We have reported on the first comprehensive *ab initio* electronic structure calculations on the quasi-two-dimensional magnetic insulators K_2NiF_4 and K_2CuF_4. They were based on density functional theory within the local density approximation and led to a convincing agreement of experiment and theory with regard to electronic, magnetic and structural properties. Moreover, we got a good insight into the interrelation of all these physical phenomena.

In particular, the almost-vanishing dispersion of the electronic structures along the z direction classified both substances as quasi-two-dimensional systems.

The transition-metal d-states corresponded quite well to a d8 and d9 configuration, respectively.

Furthermore, we stress the correct description of the insulator ground state in both compounds, since density functional theory as a ground-state theory in many cases fails to reproduce the insulator gap [38–40].

Regarding magnetism, our calculations yielded stable antiferromagnetic and ferromagnetic solutions for the Ni and Cu compound, respectively, in agreement with experiment. The magnetic moments turned out to be well localized on the transition metal sites, these being due exclusively to the d electrons. Also, their magnitude could be reproduced, albeit with deviations in the Ni case.

With respect to the structural properties we were able to confirm the measured atomic arrangements in the CuF_2 planes and particularly the in-plane distortion pattern of K_2CuF_4. This was achieved by comparing the calculated total energies at different orthorhombic distortions and by checking the band structures for a correct reproduction of the insulator gap.

Our results for K_2CuF_4 finally deviate from those of Khomskii and Kugel insofar as we *did* find a stable ferromagnetic solution for the crystal structure possessing body-centred tetragonal symmetry, as originally proposed by Knox. However, the electronic density of states calculated for this structure missed the experimentally observed gap at the Fermi energy.

According to our investigations the gap will show up only when we take both magnetic order and the orthorhombic lattice distortion into account. We therefore arrived at the

conclusion that it is the insulating ground state that requires atomic displacements and *not* ferromagnetism.

Finally, in section 4 we reported on a more detailed study of the interconnections between magnetic order, the metal–insulator transition and the orthorhombic distortion. It revealed some insight into some of the physical mechanisms and provided ground for a subsequent discussion, both in terms of itinerant and localized magnetism.

The convincing results presented in this paper should give rise to further investigations of other K_2NiF_4-type compounds, in particular the remaining systems of the K_2MF_4 series. Each of them offers its own characteristic and interesting realm of phenomena, and altogether they might provide even more insight into the physics governing magnetic and orbital instabilities [2]. However, to our knowledge, none of them has yet been investigated by first-principles electronic structure calculations.

It would be very desirable to complete the calculations presented here with the help of even more elaborate approaches. By this we mean, in particular, full-potential methods that take into account the full crystal potential, charge density and magnetization without approximations. They allow for a visualization of the latter functions and thus allow one to study their spatial distribution and their evolution in the course of orthorhombic distortions. Full-potential methods likewise enable the calculation of highly accurate total energies without the need for taking energy differences, as we had to do in this work.

These tasks are within the range of the recently developed full-potential ASW method, which has already been proven to produce quite convincing results in different areas of application, and which is now ready for use [41].

Acknowledgments

We want to thank Professor Dr P S Riseborough for fruitful discussions. This work was part of a PhD thesis of VE, accepted at the Technische Hochschule Darmstadt. It was supported by SFB 252 "Elektronisch Hochkorrelierte Metallische Materialien", Darmstadt, Frankfurt, Mainz.

References

[1] White R M 1983 *Quantum Theory of Magnetism* (Berlin: Springer)
[2] de Jongh L J and Miedema A R 1974 *Adv. Phys.* **23** 1
[3] Mermin N D and Wagner H 1966 *Phys. Rev. Lett.* **17** 1133
[4] Longo J M and Raccah P M 1973 *J. Solid State Chem.* **6** 526
[5] Mattheiss L F 1987 *Phys. Rev. Lett.* **58** 1028
[6] Anisimov V I, Korotin M A, Zaanen J and Andersen O K 1992 *Phys. Rev. Lett.* **68** 345
[7] Svane A 1992 *Phys. Rev. Lett.* **68** 1900
[8] Eyert V, Sticht J and Kübler J 1988 *Helv. Phys. Acta* **61** 496
[9] Kübler J, Eyert V and Sticht J 1988 *Physica* C **153–155** 1237
[10] Balz D 1953 *Naturwiss.* **40** 241
[11] Balz D and Plieth K 1955 *Z. Elektrochem.* **59** 545
[12] Birgeneau R J, Guggenheim H J and Shirane G 1970 *Phys. Rev.* B **1** 2211
[13] Grande B, Müller-Buschbaum H and Schweizer M 1977 *Z. Anorg. Allg. Chem.* **428** 120
[14] Ganguly P and Rao C N R 1984 *J. Solid State Chem.* **53** 193
[15] Legrand E and Plumier R 1962 *Phys. Status Solidi* **2** 317
[16] Birgeneau R J, Guggenheim H J and Shirane G 1969 *Phys. Rev. Lett.* **22** 720
[17] Skalyo J Jr, Shirane G, Birgeneau R J and Guggenheim H J 1969 *Phys. Rev. Lett.* **23** 1394
[18] Birgeneau R J, Skalyo J Jr and Shirane G 1971 *Phys. Rev.* B **3** 1736

[19] Lines M E 1967 *Phys. Rev.* **164** 736
[20] Williams A R, Kübler J and Gelatt C D Jr 1979 *Phys. Rev.* B **19** 6094
[21] Koelling D D and Harmon B N 1977 *J. Phys. C: Solid State Phys.* **10** 3107
[22] Gollisch H and Fritsche L 1978 *Phys. Status Solidi (b)* **86** 145
[23] Andersen O K 1975 *Phys. Rev.* B **12** 3060
[24] Keller J 1971 *J. Phys. C: Solid State Phys.* **4** L85
[25] Tiwari J S, Mehra A and Srivastava K G 1968 *Japan. J. Appl. Phys.* **7** 506
[26] Nolting W 1979 *Phys. Status Sol. (b)* **96** 11
[27] Yamada I 1972 *J. Phys. Soc. Japan* **33** 979
[28] Hirakawa K and Ikeda H 1973 *J. Phys. Soc. Japan* **35** 1328
[29] Ito Y and Akimitsu J 1976 *J. Phys. Soc. Japan* **40** 1333
[30] Funahashi S, Moussa F and Steiner M 1976 *Solid State Commun.* **18** 433
[31] Hirakawa K and Ubokoshi K 1981 *J. Phys. Soc. Japan* **50** 1909
[32] Hidaka M, Inoue K, Yamada I and Walker P J 1983 *Physica* B **121** 343
[33] Khomskii D I and Kugel K I 1973 *Solid State Commun.* **13** 763
[34] Kugel K I and Khomskii D I 1982 *Sov. Phys. Usp.* **25** 231
[35] Knox K 1959 *J. Chem. Phys.* **30** 991
[36] Hidaka M and Walker P J 1979 *Solid State Commun.* **31** 383
[37] Totani M, Fukuda Y and Yamada I 1989 *Phys. Rev.* B **40** 10577
[38] von Barth U 1984 *The Electronic Structure of Complex Systems* ed. P Phariseau and W Temmerman (New York: Plenum) pp 67–140
[39] Kohn W and Vashishta P 1983 *Theory of the Inhomogeneous Electron Gas* ed. S Lundquist and N H March (New York: Plenum) pp 79–147
[40] Kübler J and Eyert V 1991 *Electronic and Magnetic Properties of Metals and Ceramics* ed. K H J Buschow (Weinheim: VCH) pp 1–145
[41] Eyert V 1991 *PhD thesis* Technische Hochschule Darmstadt